

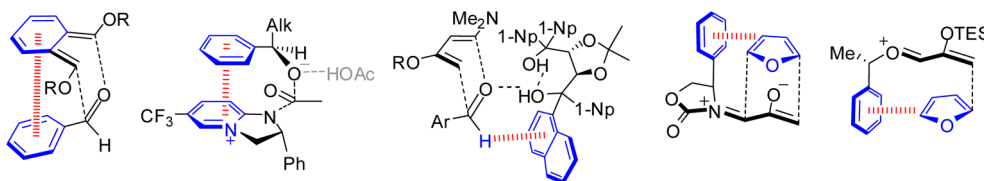
# Aromatic Interactions as Control Elements in Stereoselective Organic Reactions

ELIZABETH H. KRENSKE<sup>\*,†</sup> AND K. N. HOUK<sup>\*,‡</sup>

<sup>†</sup>*School of Chemistry, University of Melbourne, VIC 3010, Australia, and  
Australian Research Council Centre of Excellence for Free Radical Chemistry and  
Biotechnology, and* <sup>‡</sup>*Department of Chemistry and Biochemistry, University of  
California, Los Angeles, California 90095, United States*

RECEIVED ON MARCH 12, 2012

## CONSPECTUS



This Account describes how attractive interactions of aromatic rings with other groups can influence and control the stereoselectivity of many reactions. Recent developments in theory have improved the accuracy in the modeling of aromatic interactions. Quantum mechanical modeling can now provide insights into the roles of these interactions at a level of detail not previously accessible, both for ground-state species and for transition states of chemical reactions. In this Account, we show how transition-state modeling led to the discovery of the influence of aryl groups on the stereoselectivities of several types of organic reactions, including asymmetric dihydroxylations, transfer hydrogenations, hetero-Diels–Alder reactions, acyl transfers, and Claisen rearrangements.

Our recent studies have also led to a novel mechanistic picture for two classes of (4 + 3) cycloadditions, both of which involve reactions of furans with oxyallyl intermediates. The first class of cycloadditions, developed by Hsung, features neutral oxyallyl intermediates that contain a chiral oxazolidinone auxiliary. Originally, it was thought that these cycloadditions relied on differential steric crowding of the two faces of a planar intermediate. Computations reveal a different picture and show that cycloaddition with furan takes place preferentially through the more crowded transition state: the furan adds on the same side as the Ph substituent of the oxazolidinone. The crowded transition state is stabilized by a CH– $\pi$  interaction between furan and Ph worth approximately 2 kcal/mol.

Attractive interactions with aromatic rings also control the stereoselectivity in a second class of (4+3) cycloadditions involving chiral alkoxy siloxyallyl cations. Alkoxy groups derived from chiral  $\alpha$ -methylbenzyl alcohols favor crowded transition states, where a stabilizing CH– $\pi$  interaction is present between the furan and the Ar group. The cationic cycloadditions are stepwise, while the Hsung cycloadditions are concerted. Our results suggest that this form of CH– $\pi$ -directed stereocontrol is quite general and likely controls the stereoselectivities of other addition reactions in which one face of a planar intermediate bears a pendant aromatic substituent.

## 1. Introduction

Aromatic interactions ( $\pi$ -stacking, CH– $\pi$ , cation– $\pi$ , and anion– $\pi$  interactions) underpin many important structural phenomena, including conformational equilibria, molecular recognition, self-assembly, and protein–ligand binding.<sup>1</sup> Recent developments in quantum mechanical methodology have permitted increasingly accurate modeling of aromatic interactions, not only in ground-state species but also in the transition states of chemical reactions. In this Account, we show how these types of interactions are important in controlling the stereoselectivities of organic reactions.

The synthetic literature contains many examples of asymmetric reactions whose stereoselectivities changed unexpectedly upon replacement of an alkyl substituent by an aromatic group.<sup>2</sup> Although “aromatic interactions” are often invoked,<sup>3</sup> definitive evidence for their participation generally requires accurate transition-state modeling. This Account summarizes contemporary theoretical approaches that have been applied to modeling of aryl-substituent effects. Quantum mechanical modeling has shown the importance of these types of interactions in transition states and has provided explanations of a number of puzzling

phenomena. A number of new modes of stereinduction controlled by CH– $\pi$  interactions have been discovered for cycloaddition reactions. Our computations demonstrate that an aryl group can give steric attractions that lead to product distributions opposite from those that would be predicted on the basis of steric crowding.

## 2. Quantum Mechanical Calculations of Aromatic Interactions

Not all commonly used theoretical methods are well suited to the study of aromatic interactions.<sup>4</sup> Modeling of these interactions requires an accurate treatment of dispersion, a quantum mechanical phenomenon that has long posed a challenge to computation. Dispersion involves the interactions between instantaneous dipole moments in the electron distributions of two or more atoms or molecules, and calculations of dispersion-dominated systems require an adequate treatment of dynamical electron correlation.<sup>5</sup> The benchmark method for calculations of dispersion binding is coupled-cluster theory at the CCSD(T) level with extrapolation to the complete basis set limit.<sup>4,6</sup> This computationally expensive technique is currently practical only for small systems. The less expensive second-order Møller–Plesset perturbation (MP2) theory has a tendency to overestimate dispersion. Grimme's spin-component scaled MP2 variant (SCS-MP2), however, has shown very good performance.<sup>7</sup>

Density functional theory (DFT) approaches are commonly used as an alternative to wavefunction-based methods. The literature contains numerous cautionary studies highlighting the fact that many currently popular density functionals, including B3LYP,<sup>8</sup> PBE,<sup>9</sup> and PBE0,<sup>10</sup> yield serious errors for dispersion-dominated systems.<sup>4,11</sup> The failures of DFT include the prediction of too-small binding energies or even entirely repulsive interaction potentials for known bound systems. Qualitatively correct trends can sometimes be approximated artificially by use of a small basis set, since a small basis overestimates binding. However, substantial progress has been made in the development of dispersion-inclusive functionals, and a variety of economical methods are now available.

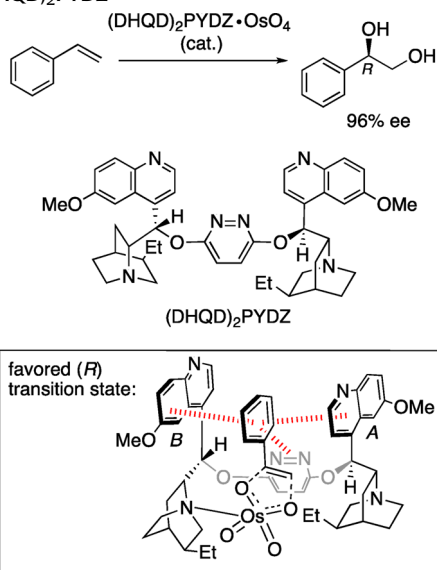
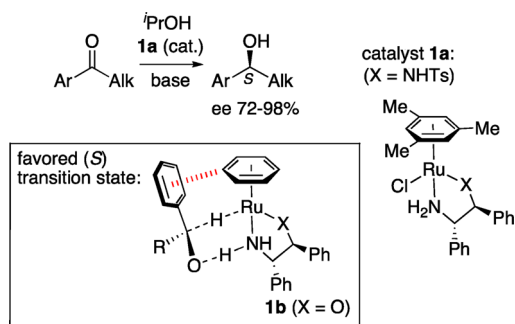
One approach has been to mimic dispersion binding by parametrizing a functional against a data set that includes noncovalent interactions. The Minnesota meta-GGA functionals developed by Truhlar<sup>12</sup> (including M05-2X and M06-2X) have attained prominence as examples of this approach. Although early M0n functionals suffered from grid-related potential energy surface oscillations,<sup>13</sup> the methods have achieved substantial popularity in the study of various dispersion-dominated systems.<sup>14</sup>

A conceptually different approach is dispersion-corrected DFT, a class of procedures often referred to as “DFT-D”.<sup>15–18</sup> Here, a conventional DFT energy is corrected by adding a term comprising the sum of individual interatomic dispersion energies, efficiently computed using a set of empirically derived dispersion coefficients. Increasingly sophisticated versions of this approach include reparametrization of the underlying functional (e.g., B97-D), virtual-orbital-dependent terms in the correlation functional (e.g., B2PLYP-D), higher-order terms, and/or hybridization-specific dispersion coefficients. Grimme's latest refinements of this approach, termed “DFT-D3”, performed superbly in benchmarking against the standard S22 data set.<sup>15b</sup> One advantage of DFT-D of relevance to organic chemists is that one can dissect the total dispersion energy of a system into separate contributions representing the interactions between particular molecular fragments.

Other approaches to the treatment of dispersion are currently being developed and should see widespread use once implemented into software packages.<sup>19</sup> The approaches mentioned above are in common use today and are illustrated by the literature examples in the following section.

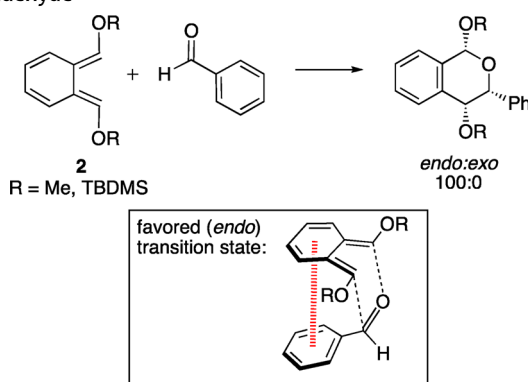
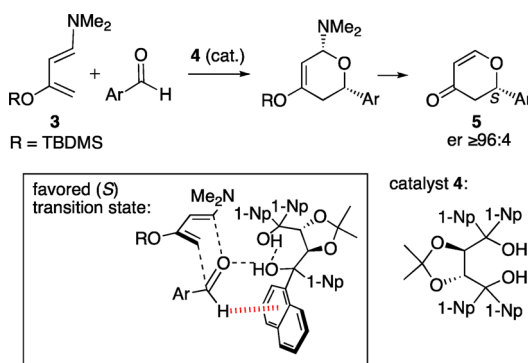
## 3. Theoretical Insights into Aromatic Interactions as Stereocontrol Elements

A relatively early example where aromatic interactions were recognized to influence stereoselectivity is the Sharpless asymmetric dihydroxylation. This reaction has been the subject of numerous computational studies, and the enantiocontrol has been explained using several different models.<sup>20</sup> In an early computational study, Maseras et al.<sup>21</sup> analyzed the asymmetric dihydroxylation of styrene, involving the chiral ligand (DHQD)<sub>2</sub>PYDZ, which coordinates OsO<sub>4</sub> and accelerates the reaction (Scheme 1). Experimentally, the *R* enantiomer of the diol is obtained in 96% ee.<sup>22</sup> Hybrid quantum mechanics/molecular mechanics calculations with IMOMM(B3LYP:MM3) suggested that the favored transition state for the stereodetermining (3 + 2) cycloaddition step has the structure shown in the box in Scheme 1. Face-to-face stacking interactions are present between the styrene Ph group and the quinoline rings of the catalyst, together with an edge-to-face interaction between Ph and the pyridazine ring. These interactions are represented by the hashed red lines. Out of the three interactions, the one involving quinoline ring A was shown to contribute approximately half of the total substrate–catalyst van der Waals interaction energy. By contrast, the corresponding interactions in the transition state leading to the minor (*S*) enantiomer were

**SCHEME 1.** Sharpless Asymmetric Dihydroxylation of Styrene, Catalyzed by (DHQD)<sub>2</sub>PYDZ<sup>21,22</sup>**SCHEME 2.** Ruthenium-Catalyzed Asymmetric Transfer Hydrogenation of Ketones<sup>23–26</sup>

only half as stabilizing. The *S* transition state is 2.7 kcal/mol higher in energy than the *R* transition state, in good agreement with the experimental enantioselectivity.

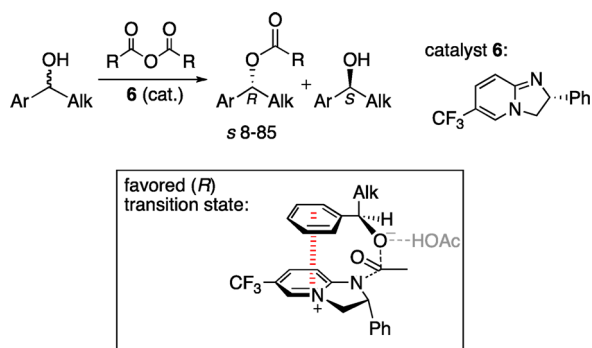
Noyori<sup>23–25</sup> uncovered the role of CH– $\pi$  interactions in transfer hydrogenations of aryl alkyl ketones catalyzed by chiral Ru( $\eta^6$ -arene) complexes (Scheme 2). Complex **1a** favored the formation of *S* alcohols with ee's of up to 98%.<sup>26</sup> Calculations on model complexes revealed a mechanism involving metal–ligand bifunctional catalysis, where the atoms of H<sub>2</sub> are transferred in a concerted fashion from a hydrido complex such as **1b**. The enantioselectivity was traced to an edge-to-face interaction between the  $\eta^6$ -arene and the aryl group on the ketone (hashed red line). The transition state shown was favored by 2.1 kcal/mol (MP2) over the less crowded enantiomeric transition state, which lacked such an interaction. The same enantiomer of the alcohol was favored if the  $\eta^6$ -benzene ligand was

**SCHEME 3.** Hetero-Diels–Alder Reactions of *o*-Xylylenes with Benzaldehyde<sup>27,28</sup>**SCHEME 4.** Asymmetric Hetero-Diels–Alder Reactions of Rawal's Diene with Aldehydes, Catalyzed by a TADDOL Derivative<sup>29,30</sup>

replaced by  $\eta^6$ -hexamethylbenzene. In this case, the stabilizing CH– $\pi$  interaction involved one of the hexamethylbenzene methyl groups rather than the arene ring itself.

Houk and Danishefsky determined that aryl–aryl stacking interactions are the stereocontrolling element in the hetero-Diels–Alder reactions shown in Scheme 3.<sup>27</sup> Experimentally, the cycloadditions of *o*-xylylenes **2** with benzaldehyde were completely *endo* selective.<sup>27,28</sup> Consistent with experiment, MP2 calculations predicted *endo* selectivities of  $\sim$ 2 kcal/mol. The *endo* transition state features a face-to-face arrangement of the two aryl groups, with an Ar–Ar separation of 3.6–3.7 Å, typical for  $\pi$ -stacking. When B3LYP calculations, lacking dispersive interactions, were applied, much smaller *endo* selectivities were predicted. The reaction of benzaldehyde with an analogous butadiene, where no aryl–aryl interaction can occur, was predicted to favor the *exo* product.

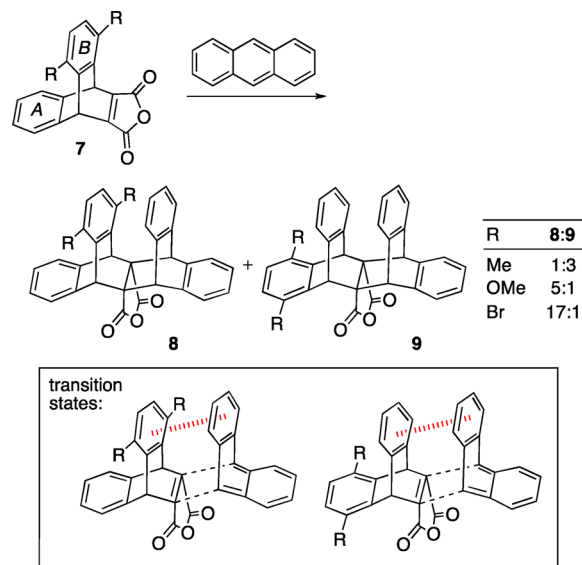
Catalytic asymmetric hetero-Diels–Alder reactions have also been found to involve aryl–aryl interactions. Rawal reported that the TADDOL derivative **4** (Scheme 4) catalyzed the cycloadditions of diene **3** with aromatic aldehydes to

**SCHEME 5.** Enantioselective Acyl Transfer Catalyzed by DHIPs<sup>32,33</sup>

afford (after workup) the (*S*)-dihydropyrones, **5**. The enantioselectivities were better than 96:4.<sup>29</sup> Computational studies<sup>30</sup> using ONIOM multilayer molecular orbital calculations (B3LYP:AM1), in conjunction with Monte Carlo conformational searching, indicated that the reaction occurs preferentially through the transition state shown in the box. The aldehyde is held in position by a combination of cooperative hydrogen bonding to the carbonyl oxygen and a CH– $\pi$  interaction (3.2 Å) between the CHO proton and the proximal naphthyl group. This transition structure was favored over the opposite enantiomer by 1.5 kcal/mol (B3LYP) or 3.4 kcal/mol (M06-2X). It was also favored by  $\geq 3$  kcal/mol over transition structures containing alternative modes of aryl–aryl interaction that had been proposed earlier by other workers.<sup>31</sup>

Birman and Houk explained the enantioselectivities of acyl transfer reactions catalyzed by 2,3-dihydroimidazo[1,2-*a*]pyridines (DHIPs) (Scheme 5).<sup>32</sup> These reactions are employed in kinetic resolutions of secondary benzylic alcohols. The DHIP **6** preferentially catalyzed the acylation of *R* alcohols, with selectivity (*s*) factors up to 85.<sup>33</sup> The preferred acylation transition state was found to have a slipped-stacked geometry. The Ar group of the alcohol is centered roughly over the pyridinium nitrogen atom (Ph–N distance 3.7 Å). This transition structure is more stable than that for acylation of the *S* alcohol, where no aryl–aryl interaction is present.

The groups of Swager and Houk<sup>34</sup> recently reported Diels–Alder reactions in which the stereoselectivity is controlled by aryl–aryl stacking interactions (Scheme 6). Cycloadditions of anthracene with dienophile **7** (R = Me, OMe, Br) furnished mixtures of the cycloadducts **8** and **9**, where the anthracene has added *syn* or *anti*, respectively, to the substituted benzene ring (*B*). The *syn/anti* ratios ranged from 1:3 (for R = Me) to 17:1 (R = Br). The product distributions were found to correlate with values of  $\Delta\Delta H^\ddagger$  computed by several density functionals. Differential aryl–aryl stacking interactions were shown to be the major stereodetermining

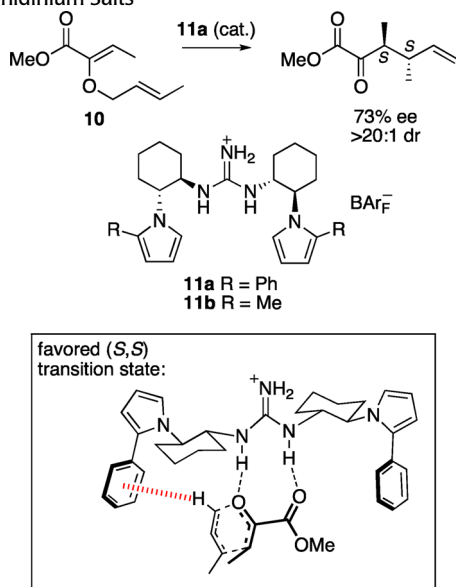
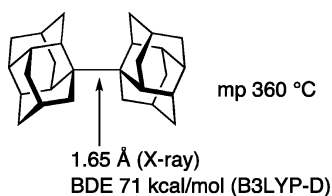
**SCHEME 6.** Diastereoselective Diels–Alder Reactions of Anthracene with Aryl-Substituted Maleic Anhydride Derivatives<sup>34</sup>

factor, and intriguingly, the stacking interaction was stronger for OMe than for Me. The substituent effects were suggested not to be due to electron density changes in the aromatic ring but to arise instead from direct through-space dispersion and electrostatic interactions between the R groups and the facing aromatic ring of the anthracene. Extensive studies of such effects by Wheeler et al.<sup>35</sup> have shown this conclusion to be quite general.

Very recently, Jacobsen<sup>36</sup> developed a theoretical model of the factors controlling enantioselectivity in catalytic asymmetric Claisen rearrangements (Scheme 7). The rearrangement of the *O*-allyl  $\alpha$ -ketoester **10**, catalyzed by chiral guanidinium salt **11a** (R = Ph), furnished the *S,S* product with 73% ee and  $>20:1$  dr. The analogous Me-substituted catalyst **11b** gave only 41% ee. Calculations with DFT and MP2 showed that two NH $\cdots$ O hydrogen bonds determine the orientation of the substrate relative to the catalyst. The *S,S* configuration is preferred because the transition state is stabilized by a CH– $\pi$  interaction (3.0 Å) between the positively charged allyl fragment and the nearby Ph group on the catalyst. This interaction is absent in the *R,R* transition state.

Although not directly related to stereoselectivity, a recent spectacular example of the role of dispersion is found in the report by Schreiner<sup>37</sup> of molecules in which bulky groups stretch CC bonds but stabilize these distorted molecules by dispersive attractive forces. The example shown in Scheme 8 has a C–C bond length of 1.65 Å yet is a crystalline solid, stable up to  $\geq 300$  °C. The C–C bond dissociation energy computed with B3LYP-D was 71 kcal/mol.

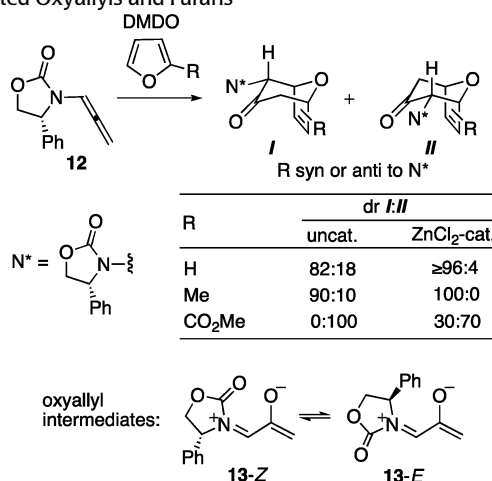
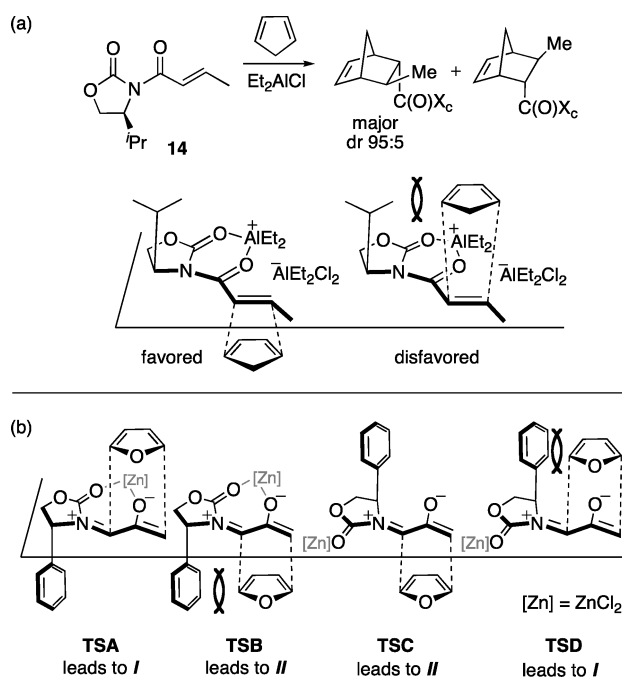


**SCHEME 7.** Enantioselective Claisen Rearrangements Catalyzed by Chiral Guanidinium Salts<sup>36</sup>**SCHEME 8.** Strained Hydrocarbon Stabilized by Dispersion Interactions

Because many of the above computational studies were performed prior to the advent of dispersion-correcting approaches,<sup>38</sup> we have re-evaluated the stereoselectivities with the B3LYP-D3 and M06-2X functionals. The Supporting Information provides a comparison of predicted stereoselectivities for the reactions in Schemes 1–7, as computed by B3LYP, B3LYP-D3, and M06-2X. The D3 correction generally increased the computed stereoselectivities for these reactions by up to 5.3 kcal/mol ( $\Delta\Delta E^\ddagger$ ), while M06-2X/6-311+G(d,p) gave smaller increases of up to 3.0 kcal/mol.

#### 4. Aromatic Interactions as Stereocontrol Elements in Oxyallyl (4 + 3) Cycloaddition Reactions

Our work has involved several different types of cycloadditions where stabilizing interactions with aryl groups favor one TS. We discovered a novel form of aryl-induced stereocontrol during collaborative work on (4 + 3) cycloaddition reactions developed by Richard Hsung.<sup>39–41</sup> The Hsung stereoselective route to 7-membered carbocycles is based on (4 + 3) cycloadditions of oxyallyls containing a chiral

**SCHEME 9.** Hsung's (4 + 3) Cycloadditions between Oxazolidinone-Substituted Oxyallyls and Furans<sup>42</sup>**SCHEME 10.** (a) Evans' Oxazolidinone-Directed Diels–Alder Reaction, Showing the Proposed Model for Stereoinduction,<sup>43</sup> and (b) Possible Transition Structures for Oxazolidinone-Directed (4 + 3) Cycloaddition Reactions

oxazolidinone.<sup>42</sup> As shown in Scheme 9, the oxyallyl is generated by oxidation of an allenamide and is trapped with a furan (or pyrrole or diene). While I and II may be formed, reactions of **12** with furan and 2-methylfuran favored cycloadduct I. The diastereomer ratios were 82:18 and 90:10, respectively, under thermal conditions and increased to ≥96:4 when ZnCl<sub>2</sub> was included in the reaction mixture. Unexpectedly, however, the reaction with methyl 2-furoate favored the opposite diastereomer, II (dr 100:0 under thermal conditions).

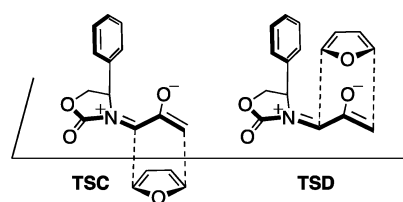
Originally, the mechanism of stereoselection in these (4 + 3) cycloadditions was thought to resemble that originally proposed by Evans<sup>43</sup> for oxazolidinone-directed Diels–Alder reactions (Scheme 10a). Evans proposed that the dienophile **14** combines with Et<sub>2</sub>AlCl to form a chelate. A diene should add most easily to the face opposite <sup>i</sup>Pr, which is less crowded.<sup>44</sup> This type of steric blocking has been invoked in many other oxazolidinone-directed reactions.<sup>45</sup> For Hsung's (4 + 3) cycloadditions, there are four analogous transition states (Scheme 10b). Cycloadduct **I** can be formed via either **TSA** or **TSD**, and cycloadduct **II** via **TSB** or **TSC**. The **I**-selectivity obtained with furan and 2-methylfuran was thought to be explained by the less-crowded **TSA**. This idea appeared to be supported by the increase in **I**-selectivity brought about by ZnCl<sub>2</sub>, which forms a chelate with the oxyallyl in **TSA**. However, this model cannot explain why a 2-CO<sub>2</sub>R substituent on the furan would lead to reversal of diastereoselectivity.

Computations at the B3LYP/6-31G(d) level indicated that only **13-E** is an energy minimum (Scheme 11). The **Z** isomer is destabilized by electrostatic repulsion between the oxygen atoms, and it collapses to the isomeric cyclopropanone

**15** upon attempted geometry optimization. Significantly, coordination to ZnCl<sub>2</sub> does not overcome the electrostatic destabilization of **13-Z**; a **Z** chelate complex does form, but it is 6.2 kcal/mol less stable than the **E** monodentate complex.

The computed transition structures for the uncatalyzed cycloaddition of **13** with furan are shown in Figure 1. The transition states that contain the **E** oxyallyl (**TSC** and **TSD**) have very low activation energies, while the **Z** transition states (**TSA** and **TSB**) are more than 15 kcal/mol higher in energy ( $\Delta\Delta H^\ddagger$ ). This is true also for the ZnCl<sub>2</sub>-catalyzed cycloaddition: coordination to ZnCl<sub>2</sub> lowers the cycloaddition barriers, but the **Z** structures remain at least 5.2 kcal/mol above the **E** structures.

Most interesting is that the addition of furan to the more crowded face of **13** (**TSD**) is favored by 0.2 kcal/mol ( $\Delta\Delta H^\ddagger$ )



	$\Delta E_{rel}^\ddagger$	
	TSC	TSD
B3LYP	0	-0.3
B3LYP <sup>a</sup>	0	-0.5
B3LYP-D	0	-1.8
B3LYP-D3	0	-2.0
B97-D	0	-2.0
M06-2X	0	-1.4
M06-2X <sup>a</sup>	0	-2.0

**FIGURE 2.** Relative energies of **TSC** and **TSD**, computed with different functionals. B3LYP/6-31G(d) geometries were used, and single-point calculations employed the 6-31G(d) basis set except for the points labeled "a", which employed the 6-311+G(d,p) basis.  $\Delta E_{rel}^\ddagger$  in kcal/mol.

**SCHEME 11.** Possible Oxyallyl Intermediates and ZnCl<sub>2</sub> Complexes

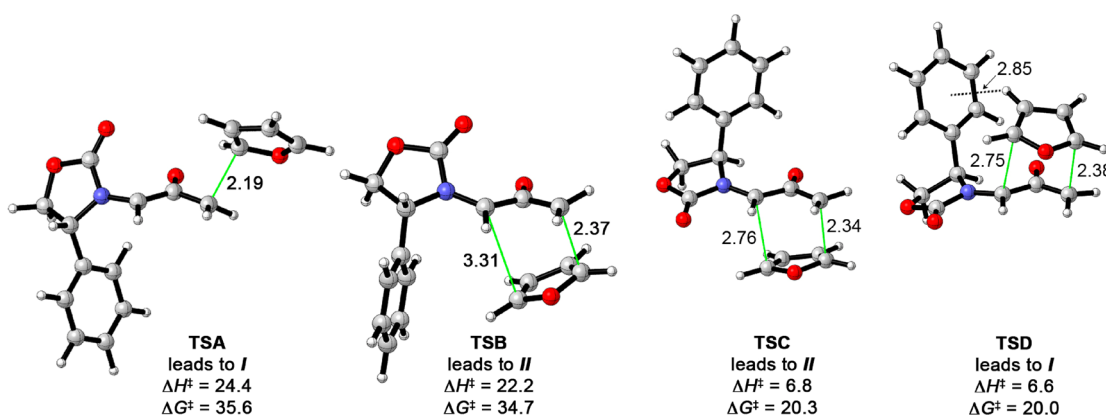
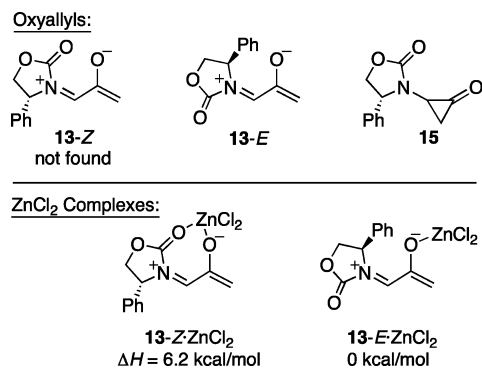


**FIGURE 1.** Transition states for the (4 + 3) cycloaddition of Hsung's oxyallyl **13** with furan (B3LYP/6-31G(d), distances in Å;  $\Delta H^\ddagger$  and  $\Delta G^\ddagger$  in kcal/mol).

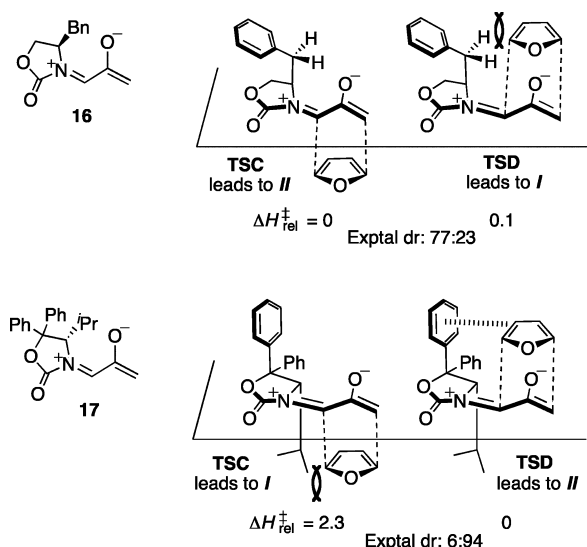


**FIGURE 3.** Experimental and calculated stereoselectivities for different oxazolidinone auxiliaries (B3LYP/6-31G(d), kcal/mol). Note: the reversed stereochemical designations for the products from **17** arise from the opposite configuration at C-4 of the oxazolidinone.

over addition to the less crowded face (**TSC**). The computed selectivity agrees with experiment and also persists when modeled in solution by means of continuum calculations with the conductor-like polarizable continuum model (CPCM).<sup>46</sup>

The 0.2 kcal/mol preference for addition to the more crowded face is traced to an edge-to-face interaction between furan and the oxazolidinone Ph substituent. In **TSD**, H-3 of the furan lies 2.85 Å from the center of the Ph ring—within the typical distance range<sup>1a</sup> for CH– $\pi$  interactions. The value of  $\Delta\Delta H^{\ddagger}$  increases to 0.6 kcal/mol when the larger 6-311+G(d,p) basis set is used, indicating that the CH– $\pi$  directed selectivity is not an artifact of basis set incompleteness. Most importantly, the stereoselectivities computed with several different dispersion-inclusive functionals give larger preferences; these results are shown in Figure 2. B3LYP-D3, B97-D, and M06-2X predict a 1.1–1.7 kcal/mol stronger stabilization of **TSD** than does B3LYP. A fragment-based analysis using B3LYP-D estimated that the interaction between furan and Ph in **TSD** is worth 2.6 kcal/mol.

The stereoselectivities involving other oxazolidinone auxiliaries were investigated, and the results are shown in Figure 3. Our predictions prompted to a definitive determination of the stereoselectivities of these reactions by X-ray crystallography. Several reassignments of stereoselectivity had to be made after it was revealed that different oxazolidinones control stereoselectivity in different ways. Replacement of the Ph group by Bn (**16**) eliminates the potential for a stabilizing CH– $\pi$  interaction in **TSD**, and a repulsive steric

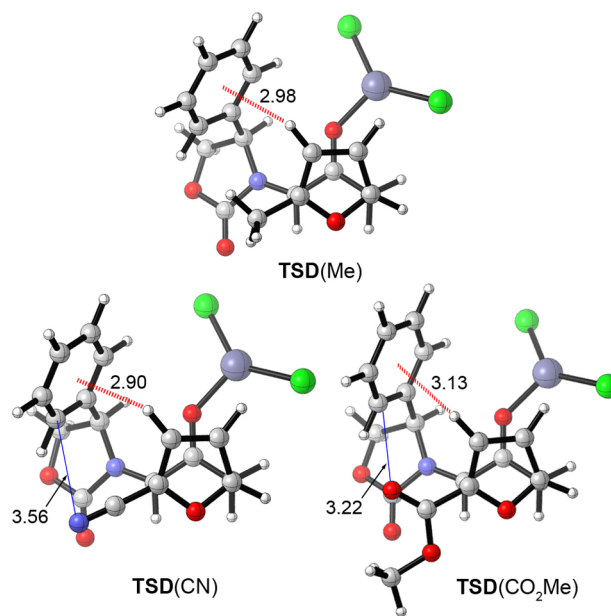
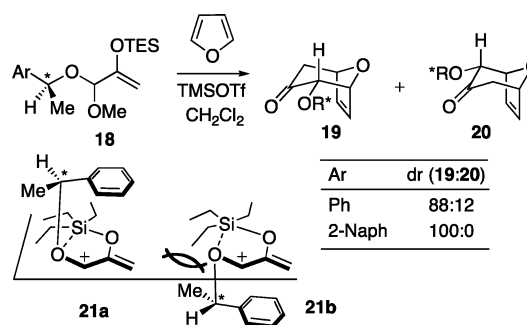


**FIGURE 4.** Top views of the transition states analogous to **TSD** for ZnCl<sub>2</sub>-catalyzed cycloadditions of **13** with 2-Me, 2-CN, and 2-CO<sub>2</sub>Me substituted furans (B3LYP/6-31G(d)+LANL2DZ, distances in Å).

**SCHEME 12.** Hoffmann's Asymmetric (4 + 3) Cycloaddition, and the Mechanism Originally Proposed To Explain the Stereocontrol<sup>47</sup>



interaction is present instead. Accordingly, the predicted selectivity reverts to favor **TSC**. Experimentally, there is a corresponding selectivity for **II** (dr 77:23). Seebach's oxazolidinone (**17**) elicits a different type of CH– $\pi$  interaction, since now the Ph group is at C-5 of the oxazolidinone. The stabilizing interaction between furan and the upper Ph group (hashed red line) acts in concert with the steric effect of the *i*Pr group on the lower face of the oxazolidinone, leading to a **II**-selectivity of 94:6. Of the two stereocontrol elements, the CH– $\pi$  interaction appears dominant, because when the two C-5 Ph groups are absent, the dr drops to only 55:45.

These calculations also rationalized the unexpected reversal of selectivity obtained with methyl 2-furoate (Scheme 9). In Figure 4 are shown transition structures analogous to **TSD** for ZnCl<sub>2</sub>-catalyzed cycloadditions of **13** with 2-Me, 2-CN, and

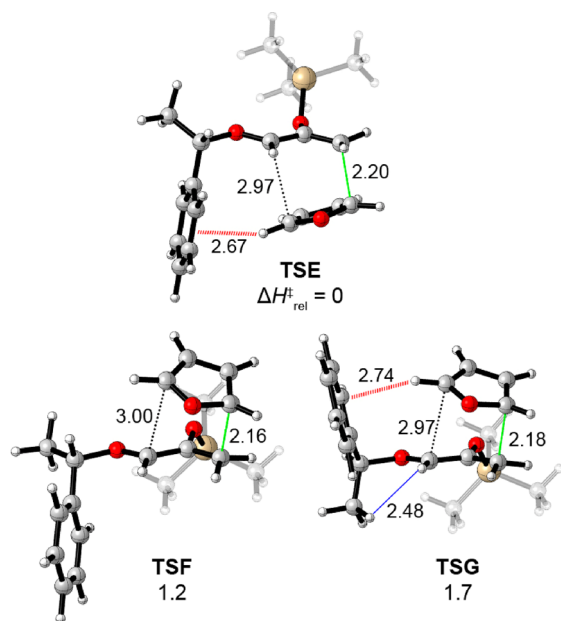


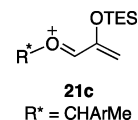
**FIGURE 5.** Transition structures for (4 + 3) cycloadditions of Hoffmann's oxyallyl cation **21** (Ar = Ph) with furan (B3LYP/6-31G(d), distances in Å,  $\Delta H^\ddagger$  in kcal/mol). The TES group was modeled by TMS.

2-CO<sub>2</sub>Me substituted furans. Each furan favors a cycloadduct in which the furan substituent lies *syn* to the oxazolidinone, but only for 2-CO<sub>2</sub>Me is **II** the major stereoisomer. A CH– $\pi$  interaction of 2.9–3.1 Å is present in each TS. For 2-CO<sub>2</sub>Me, however, electrostatic repulsion between the carbonyl oxygen and the Ph  $\pi$ -cloud results in overall destabilization. The uncrowded transition state (**TSC**) is preferred instead. The fine balance between the stabilizing CH– $\pi$  interaction and the destabilizing electrostatic repulsion is illustrated by the fact that 2-cyanofuran reacts preferentially via **TSD** to give **I**. The cyano nitrogen atom lies 0.3 Å further from the Ph  $\pi$ -cloud than does the carbonyl oxygen atom.

Our discoveries about Hsung's cycloaddition led to a re-examination of related oxyallyl cycloaddition reactions reported by H. M. R. Hoffmann (Scheme 12).<sup>47</sup> The allylic acetals **18** undergo stereoselective, Lewis acid-catalyzed (4 + 3) cycloadditions with furans to give the diastereomeric cycloadducts **19** and **20**. The stereoselectivity is determined by the configuration of the  $\alpha$ -methylbenzyl center in the alkoxy group. Diastereomer ratios ranged from 10% to 100% depending on the Ar substituent and the solvent. The best stereoselectivity was obtained with a 2-naphthyl group in CH<sub>2</sub>Cl<sub>2</sub>. Hoffmann suggested that the stereoselectivity was determined by the conformation of the intermediate oxyallyl cation. Two conformers were proposed, **21a** and **21b**. Both feature a cation– $\pi$  interaction between the allyl cation and the Ar group, and

an intramolecular RO···SiEt<sub>3</sub> interaction. Conformer **21b** would be disfavored due to steric clashing between Me and TES. Addition of furan to the less-hindered face of conformer **21a** (opposite the Ar ring) would furnish the major product.

In collaboration with Michael Harmata, we performed density functional theory calculations to examine Hoffmann's cycloaddition reactions.<sup>48</sup> B3LYP provided no evidence for the proposed Si···O-bonded intermediates **21a** and **21b**, but instead indicated that the O–R\* bond lay in the same plane as the allyl group (**21c**).



Unlike the cycloadditions of Hsung's oxazolidinone-substituted oxyallyls, Hoffmann's cycloadditions are predicted to be stepwise processes. Bond formation occurs first at the CH<sub>2</sub> terminus of the oxyallyl cation. The issue of concerted vs stepwise in this type of (4 + 3) cycloadditions has been studied previously by Cramer,<sup>49</sup> who showed that more electrophilic oxyallyl cations favor stepwise pathways. Three low-lying transition states were located for the initial bond formation (Figure 5). The lowest-energy transition state (**TSE**) corresponds to the experimental major product, while the other two transition states (**TSF** and **TSG**) both lead to the minor diastereomer.

In **TSE**, furan adds to the crowded face of the oxyallyl cation, with an edge-to-face arrangement (2.7 Å) between furan and Ph. A similar edge-to-face arrangement is present in **TSG**, but the associated stabilization is outweighed by steric repulsion between the allyl cation and Me group (blue line). **TSF** lacks any Me–H clash, but also lacks a furan–Ph interaction. When the transition states' energies are calculated with M06-2X, **TSE** remains favored overall, but **TSG** drops below **TSF** as this functional captures more strongly the stabilization associated with the CH– $\pi$  interaction.

The calculations also capture the increase in stereoselectivity observed with a 2-naphthyl group. The computed dr in the gas phase for the 2-naphthyl analogue is 95:5 by B3LYP and 99:1 by M06-2X, very close to the experimental value of 100:0. Incorporation of solvent effects by means of CPCM calculations leads to qualitative agreement with the experimental stereoselectivities in CH<sub>2</sub>Cl<sub>2</sub> and THF, and the transition-state modeling also correctly predicts regioselectivities for substituted furans such as 3-Et<sub>3</sub>Si-furan.



## 5. Conclusion

Recent advances in theoretical treatments of dispersion have provided the first density functional methods that can reliably model aromatic interactions. For synthetic chemists, these computational methods offer previously inaccessible insights into how aromatic interactions within transition states can influence stereocontrol. Given the large body of aryl-related effects on stereoselectivity that have been reported in the synthetic literature, new mechanisms of stereoinduction remain to be uncovered. Accurate theoretical modeling is also poised to allow design of new applications of aromatic interactions as stereocontrol elements. This area presents important opportunities, since aromatic interactions can enable access to different stereoselectivities from those obtained under simple steric control.

This research was supported by an NIH Grant to K.N.H. (GM-36700) and an Australian Research Council grant to E.H.K. (DP0985623).

**Supporting Information.** Comparison of predicted stereoselectivities for reactions in Schemes 1–7, and Figures 2, 3, and 5, as computed with B3LYP, B3LYP-D3, and M06-2X. This material is available free of charge via the Internet at <http://pubs.acs.org>.

## BIOGRAPHICAL INFORMATION

**Elizabeth H. Krenske** obtained her Ph.D. from the Australian National University with Professor S. B. Wild in 2005, in the area of organophosphorus and arsenic chemistry. She undertook post-doctoral studies in theoretical organic chemistry as a Fulbright Scholar with Professor Ken Houk at UCLA. Since 2009 she has been an Australian Research Council APD Fellow at the University of Melbourne.

**K. N. Houk** is the Saul Winstein Chair in Organic Chemistry at UCLA. He has published extensively on pericyclic reactions, stereoselectivity, and molecular recognition and uses the tools of computational chemistry to solve problems in organic and biological chemistry. He is a Fellow of the American Academy of Arts and Sciences and a Member of the National Academy of Sciences. This is his seventh Account.

## FOOTNOTES

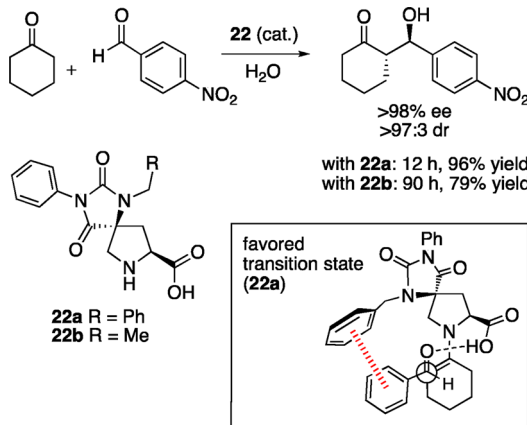
\*E-mail: [ekrenske@unimelb.edu.au](mailto:ekrenske@unimelb.edu.au); [hok@chem.ucla.edu](mailto:hok@chem.ucla.edu). The authors declare no competing financial interest.

## REFERENCES

- See, for example: (a) Nishio, M. The CH/π hydrogen bond in chemistry. Conformation, supramolecules, optical resolution and interactions involving carbohydrates. *Phys. Chem. Chem. Phys.* **2011**, *13*, 13873–13900. (b) Lehn, J.-M. *Supramolecular Chemistry: Concepts and Perspectives*; VCH: Weinheim, 1995. (c) Gillard, R. E.; Raymo, F. M.; Stoddart, J. F. Controlling Self-Assembly. *Chem.—Eur. J.* **1997**, *3*, 1933–1940. (d) Meyer, E. A.; Castellano, R. K.; Diederich, F. Interactions with Aromatic Rings in Chemical

- and Biological Recognition. *Angew. Chem., Int. Ed.* **2003**, *42*, 1210–1250. (e) Burley, S. K.; Petsko, G. A. Aromatic-Aromatic Interaction: A Mechanism of Protein Structure Stabilization. *Science* **1985**, *229*, 23–28. (f) Waters, M. L. Aromatic Interactions in Peptides. *Biopolym., Pept. Sci.* **2004**, *76*, 435–445.
- For reviews, see: (a) Nishio, M.; Hirota, M.; Umezawa, Y. *The CH/π Interaction: Evidence, Nature, and Consequences*; Wiley-VCH: New York, 1998. (b) Jones, G. B. π-Shielding in organic synthesis. *Tetrahedron* **2001**, *57*, 7999–8016. (c) Nishio, M. CH/π hydrogen bonds in organic reactions. *Tetrahedron* **2005**, *61*, 6923–6950.
  - For example, see: (a) Corey, E. J.; Matsumura, Y. Evidence for the Importance of π-π-Attractive Interactions in Enantioselective Diels–Alder Reactions Chiral Catalysts of Type (RO)<sub>2</sub>TiCl<sub>2</sub>. *Tetrahedron Lett.* **1991**, *32*, 6289–6292. (b) Ishihara, K.; Kurihara, H.; Matsumoto, M.; Yamamoto, H. Design of Brønsted Acid-Assisted Chiral Lewis Acid (BLA) Catalysts for Highly Enantioselective Diels–Alder Reactions. *J. Am. Chem. Soc.* **1998**, *120*, 6920–6930. (c) Kürti, L.; Blewett, M. M.; Corey, E. J. Origin of Enantioselectivity in the Jacobsen Epoxidation of Olefins. *Org. Lett.* **2009**, *11*, 4592–4595.
  - (a) Johnson, E. R.; Mackie, I. D.; DiLabio, G. A. Dispersion interactions in density-functional theory. *J. Phys. Org. Chem.* **2009**, *22*, 1127–1135. (b) Sherrill, C. D. Computations of Noncovalent π Interactions. In *Reviews in Computational Chemistry*; Lipkowitz, K. B., Cundari, T. R., Eds.; Wiley: New York, 2009; Vol. 26, pp 1–38. (c) Grimme, S. Density functional theory with London dispersion corrections. *WIREs Comp. Mol. Sci.* **2011**, *1*, 211–228.
  - Hartree–Fock (HF) theory fails to predict dispersion binding, because it neglects dynamical correlation.
  - (a) Jurečka, P.; Šponer, J.; Černý, J.; Hobza, P. Benchmark database of accurate (MP2 and CCSD(T) complete basis set limit) interaction energies of small model complexes, DNA base pairs, and amino acid pairs. *Phys. Chem. Chem. Phys.* **2006**, *8*, 1985–1993. (b) Takatani, T.; Hohenstein, E. G.; Malagoli, M.; Marshall, M. S.; Sherrill, C. D. Basis set consistent revision of the S22 test set of noncovalent interaction energies. *J. Chem. Phys.* **2010**, *132*, 144104.
  - Antony, J.; Grimme, S. Is Spin-Component Scaled Second-Order Møller–Plesset Perturbation Theory an Appropriate Method for the Study of Noncovalent Interactions in Molecules? *J. Phys. Chem. A* **2007**, *111*, 4862–4868.
  - (a) Lee, C.; Yang, W.; Parr, R. G. Development of the Colle–Salvetti correlation-energy formula into a functional of the electron density. *Phys. Rev. B* **1988**, *37*, 785–789. (b) Becke, A. D. A new mixing of Hartree–Fock and local density-functional theories. *J. Chem. Phys.* **1993**, *98*, 1372–1377. (c) Becke, A. D. Density-functional thermochemistry. III. The role of exact exchange. *J. Chem. Phys.* **1993**, *98*, 5648–5652.
  - Perdew, J. P.; Burke, K.; Ernzerhof, M. Generalized Gradient Approximation Made Simple. *Phys. Rev. Lett.* **1996**, *77*, 3865–3868.
  - (a) Ernzerhof, M.; Scuseria, G. E. Assessment of the Perdew–Burke–Ernzerhof exchange–correlation functional. *J. Chem. Phys.* **1999**, *110*, 5029. (b) Adamo, C.; Barone, V. Toward reliable density functional methods without adjustable parameters: The PBE0 model. *J. Chem. Phys.* **1999**, *110*, 6158.
  - See, for example: (a) Kristyán, S.; Pulay, P. Can (semi)local density functional theory account for the London dispersion forces? *Chem. Phys. Lett.* **1994**, *229*, 175–180. (b) Hobza, P.; Šponer, J.; Reschel, T. Density Functional Theory and Molecular Clusters. *J. Comput. Chem.* **1995**, *16*, 1315–1325.
  - (a) Zhao, Y.; Truhlar, D. G. The M06 suite of density functionals for main group thermochemistry, thermochemical kinetics, noncovalent interactions, excited states, and transition elements: two new functionals and systematic testing of four M06-class functionals and 12 other functionals. *Theor. Chem. Acc.* **2008**, *120*, 215–241. (b) Zhao, Y.; Truhlar, D. G. Density Functionals with Broad Applicability in Chemistry. *Acc. Chem. Res.* **2008**, *41*, 157–167.
  - Johnson, E. R.; Wolkow, R. A.; DiLabio, G. A. Application of 25 density functionals to dispersion-bound homomolecular dimers. *Chem. Phys. Lett.* **2004**, *394*, 334–338.
  - Zhao, Y.; Truhlar, D. G. Applications and validations of the Minnesota density functionals. *Chem. Phys. Lett.* **2011**, *502*, 1–13.
  - See, for example: (a) Grimme, S. Accurate Description of van der Waals Complexes by Density Functional Theory Including Empirical Corrections. *J. Comput. Chem.* **2004**, *25*, 1463–1473. (b) Schwabe, T.; Grimme, S. Double-hybrid density functionals with long-range dispersion corrections: higher accuracy and extended applicability. *Phys. Chem. Chem. Phys.* **2007**, *9*, 3397–3406. (c) Grimme, S.; Antony, J.; Ehrlich, S.; Krieg, H. A consistent and accurate ab initio parameterization of density functional dispersion correction (DFT-D) for the 94 elements H–Pu. *J. Chem. Phys.* **2010**, *132*, 154104 and references cited therein.
  - Jurečka, P.; Černý, J.; Hobza, P.; Salahub, D. R. Density Functional Theory Augmented with an Empirical Dispersion Term. Interaction Energies and Geometries of 80 Noncovalent Complexes Compared with Ab Initio Quantum Mechanics Calculations. *J. Comput. Chem.* **2007**, *28*, 555–569.
  - Liu, Y.; Goddard, W. A., III. A Universal Damping Function for Empirical Dispersion Correction on Density Functional Theory. *Mater. Trans.* **2009**, *50*, 1664–1670.

- 18 Chai, J.-D.; Head-Gordon, M. Long-range corrected hybrid density functionals with damped atom–atom dispersion corrections. *Phys. Chem. Chem. Phys.* **2008**, *10*, 6615–6620.
- 19 (a) Becke, A. D.; Johnson, E. R. Exchange-hole dipole moment and the dispersion interaction revisited. *J. Chem. Phys.* **2007**, *127*, 154108. (b) Gräfenstein, J.; Cremer, D. An efficient algorithm for the density-functional theory treatment of dispersion interactions. *J. Chem. Phys.* **2009**, *130*, 124105. (c) Kong, J.; Gan, Z.; Proynov, E.; Freindorf, M.; Furlani, T. R. Efficient computation of the dispersion interaction with density-functional theory. *Phys. Rev. A* **2009**, *79*, 042510. (d) Zhang, Y.; Xu, X.; Goddard, W. A., III. Doubly hybrid density functional for accurate descriptions of nonbond interactions, thermochemistry, and thermochemical kinetics. *Proc. Natl. Acad. Sci. U.S.A.* **2009**, *106*, 4963–4968. (e) Chai, J.-D.; Head-Gordon, M. Long-range corrected double-hybrid density functionals. *J. Chem. Phys.* **2009**, *131*, 174105. (f) Mackie, I. D.; DiLabio, G. A. Accurate dispersion interactions from standard density-functional theory methods with small basis sets. *Phys. Chem. Chem. Phys.* **2010**, *12*, 6092–6098. (g) Lee, K.; Murray, E. D.; Kong, L.; Lundqvist, B. I.; Langreth, D. C. Higher-accuracy van der Waals density functional. *Phys. Rev. B* **2010**, *82*, 081101. (h) Vydrov, O. A.; Van Voorhis, T. Implementation and assessment of a simple nonlocal van der Waals density functional. *J. Chem. Phys.* **2010**, *132*, 164113.
- 20 For a review: Drudis-Solé, G.; Ujaque, G.; Maseras, F.; Lledós, A. Enantioselectivity in the Dihydroxylation of Alkenes by Osmium Complexes. *Top. Organomet. Chem.* **2005**, *12*, 79–107.
- 21 Ujaque, G.; Maseras, F.; Lledós, A. Theoretical Study on the Origin of Enantioselectivity in the Bis(dihydroquinidine)-3,6-pyridazine-Osmium Tetroxide-Catalyzed Dihydroxylation of Styrene. *J. Am. Chem. Soc.* **1999**, *121*, 1317–1323.
- 22 Corey, E. J.; Noe, M. C. A Critical Analysis of the Mechanistic Basis of Enantioselectivity in the Bis-Cinchona Alkaloid Catalyzed Dihydroxylation of Olefins. *J. Am. Chem. Soc.* **1996**, *118*, 11038–11053.
- 23 Yamakawa, M.; Yamada, I.; Noyori, R. CH/π Attraction: The Origin of Enantioselectivity in Transfer Hydrogenation of Aromatic Carbonyl Compounds Catalyzed by Chiral  $\eta^6$ -Arene-Ruthenium(II) Complexes. *Angew. Chem., Int. Ed.* **2001**, *40*, 2818–2821.
- 24 Noyori, R.; Yamakawa, M.; Hashiguchi, S. Metal–Ligand Bifunctional Catalysis: A Nonclassical Mechanism for Asymmetric Hydrogen Transfer between Alcohols and Carbonyl Compounds. *J. Org. Chem.* **2001**, *66*, 7931–7944.
- 25 Yamakawa, M.; Ito, H.; Noyori, R. The Metal–Ligand Bifunctional Catalysis: A Theoretical Study on the Ruthenium(II)-Catalyzed Hydrogen Transfer between Alcohols and Carbonyl Compounds. *J. Am. Chem. Soc.* **2000**, *122*, 1466–1478.
- 26 (a) Hashiguchi, S.; Fujii, A.; Takehara, J.; Ikariya, T.; Noyori, R. Asymmetric Transfer Hydrogenation of Aromatic Ketones Catalyzed by Chiral Ruthenium(II) Complexes. *J. Am. Chem. Soc.* **1995**, *117*, 7562–7563. (b) Noyori, R.; Hashiguchi, S. Asymmetric Transfer Hydrogenation Catalyzed by Chiral Ruthenium Complexes. *Acc. Chem. Res.* **1997**, *30*, 97–102.
- 27 Ujaque, G.; Lee, P. S.; Houk, K. N.; Hentemann, M. F.; Danishefsky, S. J. The Origin of endo Stereoselectivity in the Hetero-Diels–Alder Reactions of Aldehydes with ortho-Xylylenes: CH–π, π–π, and Steric Effects on Stereoselectivity. *Chem.—Eur. J.* **2002**, *8*, 3423–3430.
- 28 Hentemann, M. F.; Allen, J. G.; Danishefsky, S. J. Thermal Intermolecular Hetero Diels–Alder Cycloadditions of Aldehydes and Imines via o-Quinone Dimethides. *Angew. Chem., Int. Ed.* **2000**, *39*, 1937–1940.
- 29 Huang, Y.; Unni, A. K.; Thadani, A. N.; Rawal, V. H. Single enantiomers from a chiral-alcohol catalyst. *Nature* **2003**, *424*, 146.
- 30 Anderson, C. D.; Dudding, T.; Gordillo, R.; Houk, K. N. Origin of Enantioselection in Hetero-Diels–Alder Reactions Catalyzed by Naphthyl-TADDOL. *Org. Lett.* **2008**, *10*, 2749–2752.
- 31 (a) Zhang, X.; Du, H.; Wang, Z.; Wu, Y.-D.; Ding, K. Experimental and Theoretical Studies on the Hydrogen-Bond-Promoted Enantioselective Hetero-Diels–Alder Reaction of Danishefsky's Diene with Benzaldehyde. *J. Org. Chem.* **2006**, *71*, 2862–2869. (b) Harriman, D. J.; Lambropoulos, A.; Deslongchamps, G. In silico correlation of enantioselectivity for the TADDOL catalyzed asymmetric hetero-Diels–Alder reaction. *Tetrahedron Lett.* **2007**, *48*, 689–692.
- 32 Li, X.; Liu, P.; Houk, K. N.; Birman, V. B. Origin of Enantioselectivity in CF<sub>3</sub>-PIP-Catalyzed Kinetic Resolution of Secondary Benzylic Alcohols. *J. Am. Chem. Soc.* **2008**, *130*, 13836–13837.
- 33 Birman, V. B.; Uffman, E. W.; Jiang, H.; Li, X.; Kilbane, C. J. 2,3-Dihydroimidazo[1,2-a]pyridines: A New Class of Enantioselective Acyl Transfer Catalysts and Their Use in Kinetic Resolution of Alcohols. *J. Am. Chem. Soc.* **2004**, *126*, 12226–12227.
- 34 Wheeler, S. E.; McNeil, A. J.; Müller, P.; Swager, T. M.; Houk, K. N. Probing Substituent Effects in Aryl–Aryl Interactions Using Stereoselective Diels–Alder Cycloadditions. *J. Am. Chem. Soc.* **2010**, *132*, 3304–3311.
- 35 Raju, R. K.; Bloom, J. W. G.; An, Y.; Wheeler, S. E. Substituent Effects on Non-Covalent Interactions with Aromatic Rings: Insights from Computational Chemistry. *ChemPhysChem* **2011**, *12*, 3116–3130 and references cited therein.
- 36 Uyeda, C.; Jacobsen, E. N. Transition-State Charge Stabilization through Multiple Non-covalent Interactions in the Guanidinium-Catalyzed Enantioselective Claisen Rearrangement. *J. Am. Chem. Soc.* **2011**, *133*, 5062–5075. For a relevant review, see also: Knowles, R. R.; Jacobsen, E. N. Attractive noncovalent interactions in asymmetric catalysis: Links between enzymes and small molecule catalysts. *Proc. Natl. Acad. Sci. U.S.A.* **2010**, *107*, 20678–20685.
- 37 Schreiner, P. R.; Chernish, L. V.; Gunchenko, P. A.; Tikhonchuk, E. Yu.; Hausmann, H.; Serafin, M.; Schlecht, S.; Dahl, J. E. P.; Calson, R. M. K.; Fokin, A. A. Overcoming lability of extremely long alkane carbon–carbon bonds through dispersion forces. *Nature* **2011**, *477*, 308–312.
- 38 A recent paper by Schafmeister et al. reports the asymmetric catalysis of aldol reactions in water by proline derivatives 22. The NBn derivative 22a and the NEt derivative 22b led to similar enantioselectivities and diastereoselectivities, but the rate of reaction for the Bn-substituted catalyst 22a was 44 times faster than that for Et-substituted 22b. M06-2X calculations of the transition states, optimized in water, revealed an edge-to-face interaction between the aldehyde aryl group and the Bn group in 22a. The barrier ( $\Delta G^\ddagger$ ) for 22a was 2.6 kcal/mol lower than that for 22b, in agreement with the experimental rates. See: Zhao, Q.; Lam, Y.; Kheirabadi, M.; Xu, C.; Houk, K. N.; Schafmeister, C. E. *J. Org. Chem.* **2012**, *77*, 4784–4792.



- 39 Krenske, E. H.; Houk, K. N.; Lohse, A. G.; Antoline, J. E.; Hsung, R. P. Stereoselectivity in oxallyl–furan (4 + 3) cycloadditions: control of intermediate conformations and dispersive stabilisation in cycloadditions involving oxazolidinone auxiliaries. *Chem. Sci.* **2010**, *1*, 387–392.
- 40 Lohse, A. G.; Krenske, E. H.; Antoline, J. E.; Houk, K. N.; Hsung, R. P. Regioselectivities of (4 + 3) Cycloadditions between Furans and Oxazolidinone-Substituted Oxallyls. *Org. Lett.* **2010**, *12*, 5506–5509.
- 41 Antoline, J. E.; Krenske, E. H.; Lohse, A. G.; Houk, K. N.; Hsung, R. P. Stereoselectivities and Regioselectivities of (4 + 3) Cycloadditions Between Allenamide-Derived Chiral Oxazolidinone-Stabilized Oxallyls and Furans: Experiment and Theory. *J. Am. Chem. Soc.* **2011**, *133*, 14443–14451.
- 42 (a) Xiong, H.; Hsung, R. P.; Berry, C. R.; Rameshkumar, C. The First Epoxidations of 1-Amidoallenes. A General Entry to Nitrogen-Substituted Oxallyl Cations in Highly Stereoselective [4 + 3] Cycloadditions. *J. Am. Chem. Soc.* **2001**, *123*, 7174–7175. (b) Antoline, J. E.; Hsung, R. P. An Unexpected Reversal of Diastereoselectivity in the [4 + 3]-Cycloaddition Reaction of Nitrogen-Stabilized Oxallyl Cations with Methyl 2-Furoate. *Synlett* **2008**, 739–744. (c) Lohse, A. G.; Hsung, R. P. (4 + 3) Cycloaddition Reactions of Nitrogen-Stabilized Oxallyl Cations. *Chem.—Eur. J.* **2011**, *17*, 3812–3822.
- 43 Evans, D. A.; Chapman, K. T.; Bisaha, J. Asymmetric Diels–Alder Cycloaddition Reactions with Chiral  $\alpha,\beta$ -Unsaturated N-Acyloxazolidinones. *J. Am. Chem. Soc.* **1988**, *110*, 1238–1256.
- 44 Santos et al. recently reported computational and NMR spectrometric studies suggesting a different mechanism of stereoreduction. They propose that the carbonyl groups of 14 are antiparallel and each binds one AlEt<sub>2</sub>Cl; steric hindrance from one of the AlEt<sub>2</sub>Cl groups transmits the chiral information from the oxazolidinone to the incoming diene: Bakalova, S. M.; Duarte, F. J. S.; Georgieva, M. K.; Cabrera, E. J.; Santos, A. G. An Alternative Mechanism for Diels–Alder Reactions of Evans Auxiliary Derivatives. *Chem.—Eur. J.* **2009**, *15*, 7665–7677.
- 45 Evans, D. A.; Helmchen, G.; Rüping, M. Chiral Auxiliaries in Asymmetric Synthesis. In *Asymmetric Synthesis—The Essentials*, 2nd, completely revised ed.; Christmann, M., Bräse, S., Eds.; Wiley-VCH: Weinheim, Germany, 2008; pp 3–9.
- 46 (a) Barone, V.; Cossi, M. Quantum Calculation of Molecular Energies and Energy Gradients in Solution by a Conductor Solvent Model. *J. Phys. Chem. A* **1998**, *102*, 1995–2001. (b) Cossi, M.; Rega, N.; Scalmani, G.; Barone, V. Energies, Structures, and Electronic Properties of Molecules in Solution with the C-PCM Solvation Model. *J. Comput. Chem.* **2003**, *24*, 669–681.

- 47 (a) Stark, C. B. W.; Eggert, U.; Hoffmann, H. M. R. Chiral Allyl Cations in Cycloadditions to Furan: Synthesis of 2-(1'-Phenylethoxy)-8-oxabicyclo[3.2.1]oct-6-en-3-one in High Enantiomeric Purity. *Angew. Chem., Int. Ed.* **1998**, *37*, 1266–1268. (b) Stark, C. B. W.; Pierau, S.; Wartchow, R.; Hoffmann, H. M. R. Chiral Allyl Cations Are Captured by Furan with 100% Stereoselectivity: Synthesis of Enantiopure 2-Alkoxy-8-oxabicyclo[3.2.1]oct-6-en-3-ones by Low-Temperature [4 + 3] Cycloaddition. *Chem.—Eur. J.* **2000**, *6*, 684–691.
- 48 Krenske, E. H.; Houk, K. N.; Harmata, M. Origin of Stereoselectivity in the [4 + 3] Cycloadditions of Chiral Alkoxy Siloxyallyl Cations with Furan. *Org. Lett.* **2010**, *12*, 444–447.
- 49 (a) Cramer, C. J.; Barrows, S. E. Quantum Chemical Characterization of Cycloaddition Reactions between the Hydroxyallyl Cation and Dienes of Varying Nucleophilicity. *J. Org. Chem.* **1998**, *63*, 5523–5532. (b) Cramer, C. J.; Barrows, S. E. Quantum chemical characterization of cycloaddition reactions between 1,3-butadiene and oxallyl cations of varying electrophilicity. *J. Phys. Org. Chem.* **2000**, *13*, 176–186. See also: Fernández, I.; Cossío, F. P.; de Cózar, A.; Lledós, A.; Mascareñas, J. L. Concerted and Stepwise Mechanisms in Metal-Free and Metal-Assisted [4 + 3] Cycloadditions Involving Allyl Cations. *Chem.—Eur. J.* **2010**, *16*, 12147–12157.